A Three-Dimensional Fluid-Structure Interaction Model for Platelet Aggregates Based on Porosity-Dependent Neo-Hookean Material

Yue Hao[1], Alfons G. Hoekstra[1], and Gábor Závodszky[1,2]

[1] Computational Science Lab, Informatics Institute, Faculty of Science, University of Amsterdam, Amsterdam, The Netherlands
y.hao@uva.nl
[2] Department of Hydrodynamic Systems, Budapest University of Technology and Economics, Budapest, Hungary

Abstract. The stability of the initial platelet aggregates is relevant in both hemostasis and thrombosis. Understanding the structural stresses of such aggregates under different flow conditions is crucial to gaining insight into the role of platelet activation and binding in the more complex process of clot formation. In this work, a three-dimensional implicit partitioned fluid-structure interaction (FSI) model is presented to study the deformation and structural stress of platelet aggregates in specific blood flow environments. Platelet aggregates are considered as porous mediums in the model. The FSI model couples a fluid solver based on Navier-Stokes equations and a porosity-dependent compressible neo-Hookean material to capture the mechanical characteristics of the platelet aggregates. A parametric study is performed to explore the influence of porosity and applied body force on this material. Based on *in vitro* experimental data, the deformation and associated stress of a low shear aggregate and a high shear aggregate under different flow conditions are evaluated. This FSI framework offers a way to elucidate the complex interaction between blood flow and platelet aggregates and is applicable to a wider range of porous biomaterials in flow.

Keywords: Compressible neo-Hookean · Fluid-structure interaction · Porosity · Platelet aggregate.

1 Introduction

Embolized thrombus portions can potentially block peripheral arteries, resulting in life-threatening cardiovascular diseases [3]. Platelet aggregation, the initial phase of thrombus formation, plays a vital role in thrombosis and hemostasis. The mechanical properties and morphology of platelet aggregates as well as their interaction with the flow of blood, significantly influence the further stages of aggregation and consequently the stability of the formed clot. Therefore, understanding the mechanical properties of platelet aggregates allows insight into further details of the mechanical and chemical behaviour of thrombosis, that

ICCS Camera Ready Version 2024
To cite this paper please use the final published version:
DOI: 10.1007/978-3-031-63783-4_5

might contribute to the analysis and development of treatments for thrombus [6].

Computational modelling has been used to understand the interaction between blood flow and clots [13, 25]. In the earlier works clots were considered as a rigid non-porous material [28, 24]. The importance of the porous structure of clots has been revealed in more recent studies [23, 29]. In particular, Kadria et al. [16] examined the fluid-induced shear stress imposed on the surface of thrombi using a three-dimensional blood flow simulation. However, it's essential to note that most of the prior investigations focus primarily on hemodynamics, such as blood flow velocity and fluid shear stress instead of the mechanical properties of the clot.

Experimental and computational methods have been developed and applied to quantify the mechanical behaviour of clots, including compressibility and stress response under varying forces [22, 6, 5]. Notably, the nonlinear elastic behaviour of clots has been assumed to follow neo-Hookean materials [7, 24]. Our work focuses on platelet aggregates, that represent initial stages of blood clots, constituted entirely of platelets. Platelets themselves can be characterised by a neo-Hookean constitutive model, since their defining structural component, the internal marginal band, has the behaviour of a nearly incompressible hyperelastic solid [12]. Therefore, a compressible neo-Hookean material [1] is employed to capture the mechanical properties of platelet aggregates, where the compressibility originates from the porous structure of aggregates and is dependent on porosity.

When a platelet aggregate is exposed to flow, an interaction force is exerted on the aggregates, leading to deformation. The resulting structural changes will in turn affect the fluid flow and finally reach a steady state under a constant flow condition. Generally, there are two schemes to address an FSI coupled problem, monolithic approaches or partitioned methods. With the monolithic approach, the governing equations for fluid and solid are solved simultaneously and coupling conditions at the interface are implicit in the solution procedure [4, 21]. While the partitioned method viewed fluid and solid as two subproblems individually [10, 9]. The partitioned approach can be further categorized into explicit and implicit strategies [11]. Explicit couplings solve flow and structural equations once per time step which may cause instability issues since the exact equilibrium conditions on the interface are not satisfied. Implicit techniques, on the other hand, enforce equilibrium at each time step by a coupling iteration [8]. Currently, Gauss-Seidel and Jacobi coupling schemes are the most common implicit partitioned methods [20, 30].

In this work, a partitioned FSI model is proposed to simulate and analyze the deformations and associated stress distribution inside platelet aggregates subjected to specific flow conditions. The proposed FSI model incorporates the Navier-Stokes equations to simulate blood flow, exploring the interaction forces between platelet aggregates and the surrounding fluid. Simultaneously, a compressible neo-Hookean model is employed to assess the mechanical properties of the platelet aggregates, with its compressibility determined by the poros-

ICCS Camera Ready Version 2024
To cite this paper please use the final published version:
DOI: 10.1007/978-3-031-63783-4_5

ity distribution of the aggregate. The FSI model couples these two solvers by the Gaussi-Seidel scheme. A parametric study based on the compressible neo-Hookean model is carried out to evaluate the numerical stability of the method and investigate how the porosity and applied forces impact the deformation and stress of such materials. The FSI model is subsequently applied to study the deformation and stress distribution inside the platelet aggregates at steady state under different wall shear rates (WSRs).

2 Methodology

The FSI model consists of two submodels, a fluid dynamics model for hemodynamic simulations and a hyperelastic model to simulate the response of platelet aggregate under blood flow.

2.1 Computational fluid dynamics

In the fluid dynamics model, blood flow was modelled as an incompressible Newtonian fluid governed by the Navier-Stokes equations, coupling with the Brinkman term to introduce the influence of platelet aggregate with porous structure:

$$\begin{aligned}(\mathbf{u}\cdot\nabla)\mathbf{u}-\nu\nabla^2\mathbf{u}&=\nabla p-\frac{1}{\rho}\frac{\mu}{k}\mathbf{u},\\ \nabla\cdot\mathbf{u}&=0,\end{aligned}\tag{1}$$

where $\mathbf{u}$, ν, p and μ are the flow velocity, blood kinematic viscosity, pressure and blood dynamic viscosity, respectively. In the last term on the right-hand side (Brinkman term), k represents the permeability of the platelet aggregates, which was estimated from the porosity using the Kozeny-Carman equation,

$$k=\Phi_s^2\frac{\epsilon^3 D_p^2}{150\,(1-\epsilon)^2}.\tag{2}$$

Here, Φ_s is the sphericity of the platelets, ϵ is the porosity of the aggregates and D_p represents the platelet diameter.

Table 1: **Parameter and parameter relations used in simulations.**

Notation	Description	Value	Unit	Reference
ρ	density of fluid	$1.025\ \times\ 10^{-3}$	$g\ mm^{-3}$	[26]
μ	dynamic viscosity	$3\ \times\ 10^{-3}$	$g\ mm^{-1}\ s^{-1}$	[27]
ν	kinematic viscosity	μ/ρ	$mm^{-2}\ s^{-1}$	—
Φ_s	sphericity of activated platelet	0.71	—	[18]
D_p	platelet diameter	$2\ \times\ 10^{-3}$	mm	[2]

ICCS Camera Ready Version 2024
To cite this paper please use the final published version:
DOI: 10.1007/978-3-031-63783-4_5

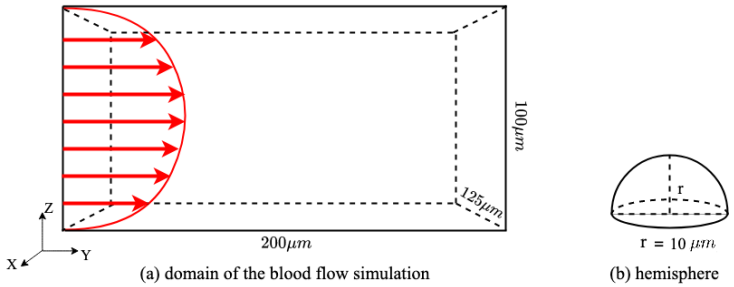

Fig. 1: Schematic diagram of the simulation domain. (a) Domain of the blood flow simulation. (b) Hemisphere used for compressible neo-Hookean materials parametric study.

The parameters used in the flow simulation and their literature sources are listed in Table 1. A cuboid domain was created to represent a blood flow channel, as shown in Fig. 1(a). The platelet aggregate was positioned on the bottom wall of the domain. The blood flowed through the domain along the positive y direction. As the blood flow domain represented a small part of the experimental channel in the x direction, consistent velocity profiles were assigned in the x direction, while parabolic profiles were designated in the z direction at the inlet. At the outlet, a constant pressure condition was prescribed. No-slip boundary conditions were imposed at the top and bottom walls.

2.2 Porosity-dependent compressible neo-Hookean materials

Platelet aggregates are not rigid bodies and can deform when subjected to the forces of blood flow. The force exerted on the porous structure in flow can be described using permeability as:

$$f = \frac{\mu}{k}\mathbf{u}. \tag{3}$$

This force can subsequently be interpreted as external body force for the mechanical model of the platelet aggregate to explore deformation and compression of the aggregate under flow.

We consider the platelet aggregates as a porous media characterized by compressible neo-Hookean model. Suppose that the aggregate is subjected to the displacement field $\mathbf{D}$, the deformation gradient can be written as $\mathbf{F} = \partial\mathbf{x}/\partial\mathbf{X}$ where $\mathbf{X}$ denotes the position of the aggregate in the reference configuration, while $\mathbf{x} = \mathbf{X} + \mathbf{D}$ is the corresponding deformed configuration of such aggregate. The strain energy density function of a compressible neo-Hookean material, W, is a scalar function of the right Cauchy-Green strain tensor $\mathbf{C} = \mathbf{F}^T\mathbf{F}$:

$$W = \frac{G}{2}(I_1 - 3) - G\ln[J] + \frac{\lambda}{2}(\ln[J])^2, \tag{4}$$

ICCS Camera Ready Version 2024
To cite this paper please use the final published version:
DOI: 10.1007/978-3-031-63783-4_5

where G denotes the shear modulus, λ denotes the Láme coefficient, $I_1 = tr(\mathbf{C})$ is the first invariant of $\mathbf{C}$, and $J := det\mathbf{F}$ represents the volume change. In simulations, the shear modulus G of the platelet aggregates was chosen to be 1000 Pa [15].

Compared to the standard neo-Hookean materials, this porous neo-Hookean material has an effective Young's modulus E,

$$E = \frac{3G}{1 + \frac{1}{2}\epsilon^2}, \tag{5}$$

and an effective Possion's ratio v,

$$v = \frac{1 - \epsilon^2}{2 + \epsilon^2}. \tag{6}$$

Then the Láme coefficient λ is given by:

$$\lambda = \frac{Ev}{(1 + v)(1 - 2v)}. \tag{7}$$

These material properties depend on the porosity ϵ of the material, which introduces the porosity-dependent compressibility to the porous structures [19]. Notably, a highly porous material exhibits an effective Poisson ratio approaching zero, as well as an effective Young's modulus tending toward $2G$. Conversely, a material with low porosity has $v \to \frac{1}{2}$ and $E \to 3G$, aligning with the expected behaviour of an incompressible neo-Hookean solid.

After a single run of the compressible neo-Hookean material simulation, the material undergoes deformation and compression, resulting in consequential changes to its porosity. The change of the porosity due to deformation is quantified by the volumetric strain, $\mathrm{div}(\mathbf{d})$, where $\mathbf{d}$ denotes the displacement. The updated porosity is then computed by

$$\epsilon' = \frac{\mathrm{div}(\mathbf{d}) + \epsilon}{\mathrm{div}(\mathbf{d}) + 1}. \tag{8}$$

Such variation of porosity may lead to changes in the local mechanical properties and result in further deformation. Therefore, we iteratively update the corresponding porosity and repeat the simulation until the material configuration reaches a steady state.

To quantify the stress distribution inside the aggregates, the Von Mises stress σ_v, which can be derived by the Cauchy stress tensor σ, is calculated:

$$\sigma_v = \sqrt{\frac{1}{2}\left[(\sigma_{11} - \sigma_{22})^2 + (\sigma_{22} - \sigma_{33})^2 + (\sigma_{33} - \sigma_{11})^2\right] + 3\,(\sigma_{12}^2 + \sigma_{23}^2 + \sigma_{31}^2)}. \tag{9}$$

where σ_{ij} denotes the element of Cauchy stress tensor.

ICCS Camera Ready Version 2024
To cite this paper please use the final published version:
DOI: 10.1007/978-3-031-63783-4_5

2.3 The fluid-structure coupling

An implicit partitioned FSI method is applied to couple the flow solver (section 2.1) and the structural solver (section 2.2). Platelet aggregate are considered as a porous medium attached to the channel wall. The aggregate will deform under the influence of hemodynamics, and correspondingly, the deformed configurations of the aggregate will result in a change in hemodynamics. Applying an implicit partitioned approach, an equilibrium state between fluid and structure should be reached. Note that, different from traditional FSI problem, there is no explicit interface between flow and structure but the entire structure is immersed in the fluid and exposed to the stresses. The flow solver can be viewed as a function of the configuration of the platelet aggregate,

$$f = \mathcal{F}(\mathbf{x}), \tag{10}$$

where f denotes the corresponding interaction kinetic force the platelet aggregate subjected to. Similarly, the structural solver is considered as a position function of the interaction force:

$$\mathbf{x} = \mathcal{S}(f). \tag{11}$$

The FSI problem therefore can be formulated as a root-finding problem such that the difference between the presumed configuration of the solid and the resulting one after FSI computation is minimised:

$$\arg\min_{\mathbf{x}} ||\mathcal{S} \circ \mathcal{F}(\mathbf{x}) - \mathbf{x}||. \tag{12}$$

The solution to the root-finding problem leads the presumed configuration to converge to the desired configuration in the equilibrium state. In our cases, $\mathcal{S} \circ \mathcal{F}(\mathbf{X})$ was employed as the initial guess of the presumed configuration. Given this initial guess, a Gauss-Seidel iteration scheme [20] updates the presumed configuration every step by minimizing the objective function Eq. 12 and the Aitken relaxation factor ω is adopted to accelerate the convergence [17], as shown in Algorithm 1.

It is noteworthy that due to the deformation of the platelet aggregate, the corresponding porosity and its position will be changed as well in the fluid domain. Therefore extra interpolations between the solid domains and the fluid domain are required. We present the detailed schematic workflow of one iteration (step 4 to 11 in Algorithm 1) of this FSI model in Fig. 2. The updated presumed position computed every iteration will affect the flow solver from two aspects: new geometry of the platelet aggregate and changes in porosity due to deformation and compression. First, the porosity position in the fluid domain has to be updated as the configuration of the platelet aggregate alters. Second, the deformation and compression of the geometries will result in the variation of porosity and subsequently influence the corresponding permeability. Therefore the new permeability information on the flow domain has to be interpolated from a deformed solid model based on the updated presumed configuration before simulation. The flow solver estimates the kinetic force applied on the porous

ICCS Camera Ready Version 2024
To cite this paper please use the final published version:
DOI: 10.1007/978-3-031-63783-4_5

Algorithm 1 The Gauss-Seidel iteration scheme with Aitken relaxation factor

Input: Flow solver $\mathcal{F}$, structural solver $\mathcal{S}$, stopping criteria ϱ, initial presumed configuration $\mathbf{x}^0$, initial Aitken relaxation factor ω^0.
Output: Converged configuration $\mathbf{x}^*$

$n = 0$
$\tilde{\mathbf{x}}^0 = \mathcal{S} \circ \mathcal{F}\left(\mathbf{x}^0\right)$
$\boldsymbol{r}^0 = \tilde{\mathbf{x}}^0 - \mathbf{x}^0$
while $\|\boldsymbol{r}^n\|_2 > \varrho$ **do**
    $n++$
    $\mathbf{x}^n = \mathbf{x}^{n-1} + \omega^{n-1}\boldsymbol{r}^{n-1}$
    $\tilde{\mathbf{x}}^n = \mathcal{S} \circ \mathcal{F}\left(\mathbf{x}^n\right)$
    $\boldsymbol{r}^n = \tilde{\mathbf{x}}^n - \mathbf{x}^n$
    $\omega^n = -\omega^{n-1}\frac{(\boldsymbol{r}^{n-1})^T(\boldsymbol{r}^n - \boldsymbol{r}^{n-1})}{(\boldsymbol{r}^n - \boldsymbol{r}^{n-1})^T(\boldsymbol{r}^n - \boldsymbol{r}^{n-1})}$
end while
$\mathbf{x}^* = \mathbf{x}^n$

medium and hands the information to the solid solver, considering it as body force. The solid solver resolves the corresponding displacement induced by this body force and quits the loop if the residual between the presumed and actual configuration is small enough.

Tetrahedral meshes were employed for both CFD and platelet aggregate meshes. The resolution of CFD meshes was refined to enhance accuracy specifically in the region surrounding the platelet aggregate. The model was implemented via FreeFEM [14] and performed on the Dutch national supercomputer Snelllius (SURF, The Netherlands) on 64 AMD Rome 7H12 CPU $\times 2$ cores.

3 Results

3.1 Compressible neo-Hookean parametric study

Before we implement the FSI model, a parametric study of porosity-dependent neo-Hookean materials was performed to investigate the influence of the porosity and the applied force on the deformation stress of materials. A hemisphere with a radius of 10 µm, was employed as a simplified configuration of aggregates. Homogeneous porosity was assigned to the hemisphere and a constant body force in the y-direction was applied.

The results of the parametric study are demonstrated in Fig. 3. The increase in magnitude of the body force leads to a larger average and maximum displacement and volumetric strain. Similarly, with the increase of the porosity, the average displacement also increases. However, compared with the influence of body force on the displacement, the effect of porosity on it is less significant. An interesting phenomenon can be observed from the change of the porosity in Fig. 3(c). The porosity change demonstrates a non-monotonic trend across various initial porosity values, with the largest occurring when the initial porosity equals 0.5. A potential reason for this behaviour is elaborated in the *Discussion*

ICCS Camera Ready Version 2024
To cite this paper please use the final published version:
DOI: 10.1007/978-3-031-63783-4_5

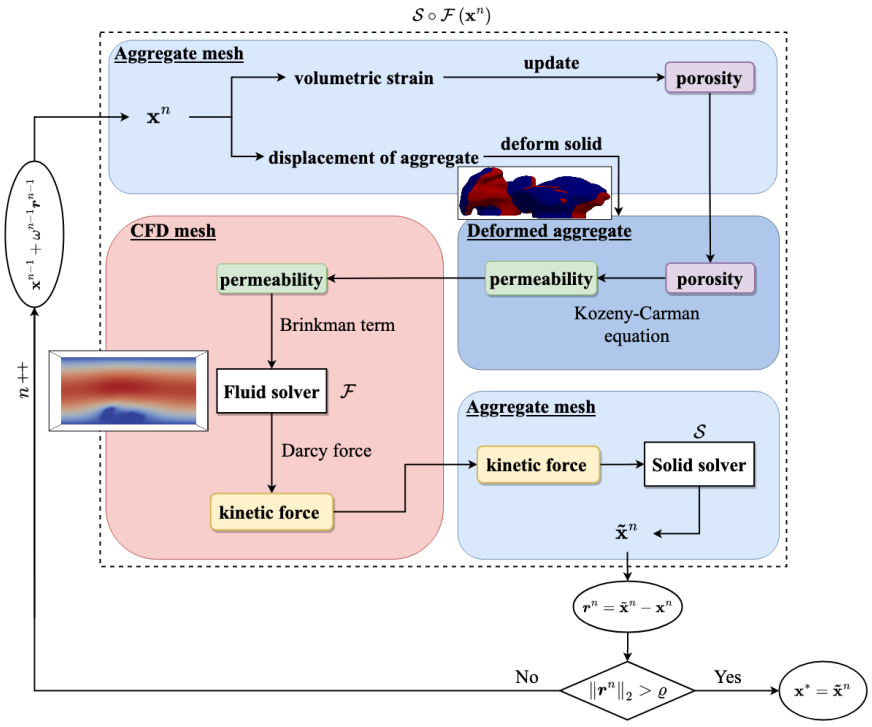

Fig. 2: Flow diagram for one iteration (step 4 to 11 in Algorithm 1) of the FSI model. The blocks in red, light blue, darker blue color represent the computational fluid dynamic (CFD) mesh, reference aggregate mesh and deformed aggregate mesh, respectively. The information shown on the blocks includes the data saved on this mesh and the operation performed based on this mesh.

section. Notably, although the average change of porosity is small, the maximum porosity change among all cases reaches 0.152, approximately 30% of the corresponding initial porosity value.

Fig. 4 shows the distribution of von Mises stress obtained from varying body forces and different porosity. An increase in body force leads to higher stress levels within the hemisphere. In the lower porosity cases, the object tends to behave more like an incompressible solid, therefore the ratio of high stress inside the hemisphere increases.

The deformation, porosity before and after deformation and stress distribution within the hemisphere subjected to a 5×10^{-5} N/µm^3 body force and an initial porosity of 0.9 (case with the most significant displacement) are presented in Fig. 5. Since the applied body force acts in the y-direction, it is observed that the hemisphere undergoes a noticeable deformation towards the positive y-direction. This deformation leads to stretching around the left bottom edge of the hemisphere and compression around the right bottom edge. Consequently,

ICCS Camera Ready Version 2024
To cite this paper please use the final published version:
DOI: 10.1007/978-3-031-63783-4_5

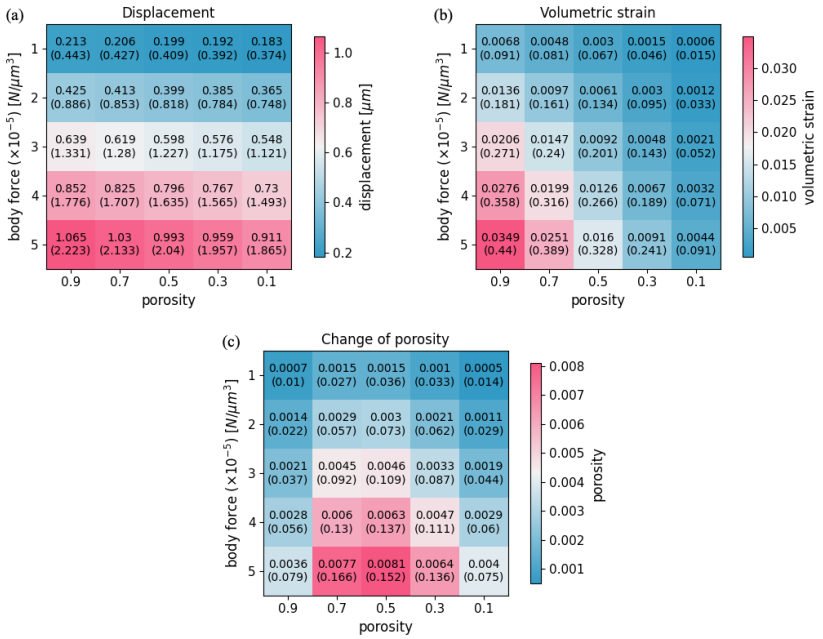

Fig. 3: Parametric study of the effect of deformation. (a) Heatmap of displacement, (b) volumetric strain, and (c) change of porosity of the porosity-dependent compressible neo-Hookean materials. The average values are shown on the heatmap, with the maximum values shown in brackets. The color corresponds to the magnitude of the average value.

the porosity of the left bottom part increases, while the bottom right part of the hemisphere becomes denser. On the right bottom edge, the porosity has decreased to 0.82. Moreover, Fig. 5(d) demonstrates the von Mises stress distribution inside the hemisphere on a cross-section. The high stress region is distributed at the lower part of the hemisphere close to the immovable base.

3.2 FSI simulation

We applied the proposed FSI model to both low shear and high shear aggregate data as obtained in earlier experiments [13]. In the low shear aggregate case the maximum inlet flow velocity was set to 20 mms^{-1}, corresponding to the flow condition of 800 $^{-1}$ WSR. For the high shear cases the maximum inlet flow velocities of 40 mm s^{-1} and 100 mm s^{-1}were prescribed. These velocities correspond to WSRs of 1600 s^{-1} and 4000 s^{-1} flow environments, respectively.

The original configuration, the deformed configuration, and the comparison of them under WSR = 4000 s^{-1} flow are presented in Fig. 6(a). The aggregate deformed visibly along the direction of blood flow (positive y-direction). A noticeable difference between the reference and deformed configurations can

ICCS Camera Ready Version 2024
To cite this paper please use the final published version:
DOI: 10.1007/978-3-031-63783-4_5

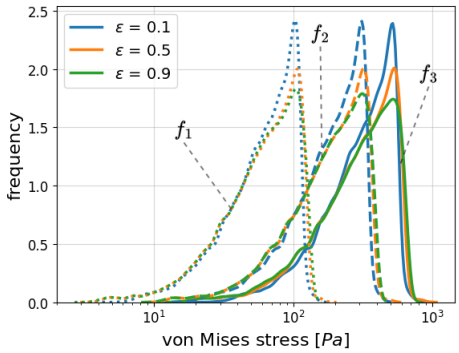

Fig. 4: Distribution of von Mises stress inside the hemispheres with a porosity of 0.1, 0.5 and 0.9 in log-scale. $f_1 = 1 \times 10^{-5}$ N/µm^3, $f_2 = 3 \times 10^{-5}$ N/µm^3 and $f_3 = 5 \times 10^{-5}$ N/µm^3.

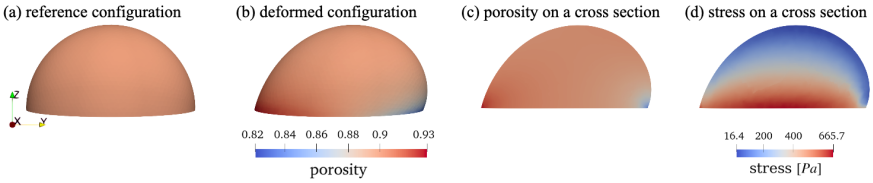

Fig. 5: (a),(b) - Reference configuration and deformed configuration of the hemisphere. The color represents the porosity on it. (c), (d) - Porosity and von Mises stress on a cross-section of the deformed hemisphere.

be observed in the comparison figure. Furthermore, it is important to evaluate the the stress within the platelet aggregate, since it might be connected to the platelet activation and the stability of such aggregate. Fig. 6(b) demonstrates the von Mises stress distribution on a cross-section of the deformed configuration of the same aggregate. As expected, the stress close to the attachment region (bottom) of the aggregates is higher than that on the top part.

Effect of increasing WSR. With the increase of WSR, both the strain and the vom Mises stress of the aggregates becomes more significant (see Table 2, two-way). The maximum displacement of the low shear aggregate is 0.145 µm, while that for high shear aggregate under a flow condition of 4000 s^{-1} WSR reaches 3.91 µm. This is a result of the larger forces induced by the high flow velocity. Moreover, the maximum von Mises stress is almost two orders of magnitude greater under high WSR compared to values of low WSR flow conditions, increasing from 43.46 Pa to 1263.3 Pa.

Comparison of two-way coupled FSI with one-way coupled FSI simulation. A comparison between the results of two-way coupled FSI and one-way

ICCS Camera Ready Version 2024
To cite this paper please use the final published version:
DOI: 10.1007/978-3-031-63783-4_5

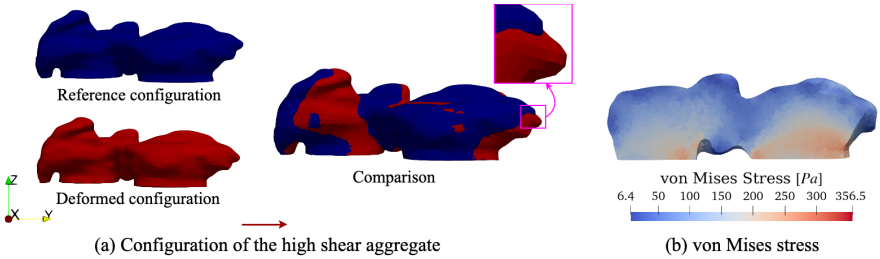

Fig. 6: (a) The reference configuration, deformed configuration and comparison of them under a WSR = 4000 s^{-1}. The reference configuration is represented in blue color, while the deformed configuration is represented in red. The appearance of red in the comparison figure signifies a difference of the aggregate surfaces due to deformation. The small box in the comparison figure is a zoom-in figure showing the differences between the two configurations. The red arrow indicates the direction of blood flow. (b) Von Mises stress distribution on a cross-section of the deformed platelet aggregate under WSR = 4000 s^{-1} flow conditions.

coupled FSI simulation is presented in Table 2. It is observed that across all factors of interest, the results obtained from one-way coupled FSI simulation exhibit smaller values compared to the results of two-way coupled FSI model. This disparity between the two models becomes more pronounced with increasing WSRs. Specifically, while the average displacement disparity remains relatively minimal at low shear conditions, approximately 0.01 µm, it increases to 0.31 µm under a WSR of 4000 s^{-1}. Similar trends can be observed in stress and porosity variations. In the scenario of high shear aggregate under a flow condition of 4000 s^{-1} WSR, the discrepancy observed in maximum stress for the two models amounts to approximately 200 Pa. Conversely, under a low WSR condition, this difference diminishes significantly to one-twentieth of its counterpart in the high WSR scenario.

Furthermore, it is noteworthy that the maximum porosity variation observed for the low shear aggregate and the high shear aggregate under a shear rate of 1600 s^{-1} remains below 0.1 for both two-way and one-way coupled FSI models, with an average value of less than 0.01. Such minor changes suggest that they are unlikely to exert a significant influence on the porous structure of the aggregate. In contrast, noticeable porosity changes are evident for the high shear aggregate subjected to a shear rate of 4000 s^{-1} in both two-way and one-way coupled FSI models, with a disparity of two models approximately 0.02.

4 Discussion

This work presents a novel methodology for modelling the interaction between platelet aggregates and hemodynamics under specific flow conditions. The model incorporates a fluid solver based on the Navier-Stokes equation to simulate hemodynamics and a porosity-dependent compressible neo-Hookean material to sim-

ICCS Camera Ready Version 2024
To cite this paper please use the final published version:
DOI: 10.1007/978-3-031-63783-4_5

Table 2: **Comparason of two-way coupled FSI with one-way coupled FSI simulation results.**

	d_{avg} $[\mu m]$	$d_{\max}$ $[\mu m]$	$\sigma_{v,\text{avg}}$ $[Pa]$	$\sigma_{v,\max}$ $[Pa]$	$\lvert\Delta\epsilon\rvert_{\text{avg}}$ $(\times 10^{-4})$	$\lvert\Delta\epsilon\rvert_{\max}$
Low shear aggregate under WSR = 800 s^{-1}						
two-way	0.042 ± 0.027	0.145	9.60 ± 3.22	43.46	3.3 ± 3.2	0.0061
one-way	0.031 ± 0.021	0.118	6.90 ± 2.78	33.48	2.5 ± 2.5	0.0047
High shear aggregate under WSR = 1600 s^{-1}						
two-way	0.556 ± 0.029	1.60	44.33 ± 25.22	474.5	2.20 ± 2.33	0.080
one-way	0.423 ± 0.232	1.351	33.28 ± 20.20	393.4	1.76 ± 1.76	0.075
High shear aggregate under WSR = 4000 s^{-1}						
two-way	1.388 ± 0.730	3.91	108.8 ± 63.95	1263.3	7.38 ± 6.38	0.185
one-way	1.079 ± 0.601	3.47	84.77 ± 51.89	1074.29	5.74 ± 4.75	0.165

Average displacement magnitude (d_{avg}), maximum displacement magnitude ($d_{\max}$), average von Mises stress ($\sigma_{v,\text{avg}}$), maximum von Mises stress ($\sigma_{v,\max}$), average porosity change ($|\Delta\epsilon|_{\text{avg}}$), and maximum porosity change ($|\Delta\epsilon|_{\max}$) of low shear aggregate under a WSR of 800 s^{-1}, high shear aggregate under a WSR of 1600 s^{-1} and high shear aggregate under a WSR of 4000 s^{-1} flow conditions.

ulate aggregate deformation. Platelet aggregates are considered as porous mediums and the corresponding porosity varies along with volumetric strain under deformation. The proposed FSI model provides a more precise and effective way to simulate the behavior of aggregates.

The parametric study of porosity-dependent compressible neo-Hookean materials elucidate the material behavior including the variation of porosity, stress distribution and deformation under different magnitude of body forces and initial porosity. Both the initial porosity and the magnitude of the body force have a positive correlation with material deformation. Varying the initial porosity also leads to different stress distributions within the materials. A non-monotonic relation was observed between the average change of the porosity and the magnitude of initial porosity (see Fig. 3(c), maximum at $\epsilon = 0.5$). An intuitive explanation to this phenomenon is that the change in porosity is not only a function of volumetric strain but also its initial porosity, e.g. $|\Delta\epsilon| = |(\epsilon - 1)\frac{\text{div}(\mathbf{d})}{1+\text{div}(\mathbf{d})}|$, therefore the change of porosity will be scaled by its initial porosity despite a monotonic tendency of volumetric strain observed along with the increase of the initial porosity.

The results of the FSI model reveal that noticeable deformation only occurs in very high WSR flow conditions. Within low WSR environments, the difference in deformation between the two-way and one-way FSI models is negligible,

ICCS Camera Ready Version 2024
To cite this paper please use the final published version:
DOI: 10.1007/978-3-031-63783-4_5

which suggests that one-way FSI may be preferred over the two-way model for these cases considering the computational cost. Furthermore, the peak of the structural stress inside the aggregates increases with the increase of the WSR. This phenomenon can be attributed to two potential factors. On the one hand, faster flow will result in higher forces as shown in Eq. 3, and on the other hand, the geometry of the high shear aggregates tends to grow taller, protruding more into the flow and therefore will interact with the flow regions of higher velocity. However, it is shown in [15] that the shear modulus can change with the applied stress, and the accuracy of this shear modulus directly affects the magnitude of deformation. Therefore further investigations are required to evaluate precise material parameters under different flow conditions. By leveraging configuration data of aggregates measured from blood perfusion experiments with and without blood flow force, the shear modulus can be inferred by formulating an inverse problem. The obtained shear modulus can subsequently serve as a parameter in FSI model to simulate the behaviour of aggregates over time under different flow environments.

Although the proposed model demonstrates notable effectiveness, it is crucial to acknowledge its limitations. First, since an additional pressure term needs to be introduced to supplement the Cauchy stress in an incompressible material, setting $\epsilon = 0$ might result in numerical instabilities in the porosity-dependent compressible neo-Hookean materials. In this study, for numerical stability 0.01 was chosen as the minimum value for porosity which only introduces a negligible error. Moreover, since the FSI model is coupled by an implicit partitioned scheme, the fluid and solid solver are called repeatedly and may lead to high computational costs. To reduce the necessary computational resources, an adaptive mesh was generated for the CFD simulations. The mesh was refined at the position of aggregates to cope with the potential complexity of fluid dynamics while remaining relatively coarse away from the aggregate. This refinement enhances the accuracy of interaction forces derived from the CFD simulations, thereby improving the fidelity of input data for the neo-Hookean materials model. Furthermore, the interpolations between meshes in the Gauss-Seidel iteration will inevitably introduce discrepancies to the model and propagate. This error can be reduced by employing finer meshes at the cost of increased computational effort.

5 Conclusion

In this work, we present an FSI model to simulate and investigate platelet aggregate deformation and associated stress under three different flow conditions based on porosity-dependent compressible neo-Hookean materials. A parametric analysis of neo-Hookean materials highlights the importance of porosity on deformation and stress. The proposed FSI model incorporates the internal microstructure of the aggregates and facilitates a relatively precise prediction of the aggregate deformation stress in specific flow environments. The results suggests that employing a high-detail mechanical model is advantageous mostly

ICCS Camera Ready Version 2024
To cite this paper please use the final published version:
DOI: 10.1007/978-3-031-63783-4_5

under elevated flow conditions. Finally, this work lays a foundation for a better understanding of the deformability and mechanical properties of the platelet aggregates, which in turn could be used in the prediction of the stability of platelet aggregates or more complex porous biomaterials in the future.

References

1. Barsimantov, J., Payne, J., de Lucio, M., Hakim, M., Gomez, H., Solorio, L., Tepole, A.B.: Poroelastic characterization and modeling of subcutaneous tissue under confined compression. Annals of Biomedical Engineering (Mar 2024)
2. Bath, P., Butterworth, R.: Platelet size: measurement, physiology and vascular disease. Blood coagulation & fibrinolysis : an international journal in haemostasis and thrombosis **7**(2), 157—161 (March 1996)
3. Bershadsky, E.S., Ermokhin, D.A., Kurattsev, V.A., Panteleev, M.A., Nechipurenko, D.Y.: Force balance ratio is a robust predictor of arterial thrombus stability. Biophysical Journal (2024)
4. Blom, F.J.: A monolithical fluid-structure interaction algorithm applied to the piston problem. Computer Methods in Applied Mechanics and Engineering **167**(3), 369–391 (1998)
5. Boodt, N., van Schauburg, P.R.S., Hund, H.M., Fereidoonnezhad, B., McGarry, J.P., Akyildiz, A.C., van Es, A.C., Meyer, S.F.D., Dippel, D.W., Lingsma, H.F., van Beusekom, H.M., van der Lugt, A., Gijsen, F.J.: Mechanical characterization of thrombi retrieved with endovascular thrombectomy in patients with acute ischemic stroke. Stroke **52**(8), 2510–2517 (2021)
6. Cahalane, R.M.E., de Vries, J.J., de Maat, M.P.M., van Gaalen, K., van Beusekom, H.M., van der Lugt, A., Fereidoonnezhad, B., Akyildiz, A.C., Gijsen, F.J.H.: Tensile and compressive mechanical behaviour of human blood clot analogues. Annals of Biomedical Engineering **51**(8), 1759–1768 (Aug 2023)
7. van Dam, E.A., Dams, S.D., Peters, G.W.M., Rutten, M.C.M., Schurink, G.W.H., Buth, J., van de Vosse, F.N.: Non-linear viscoelastic behavior of abdominal aortic aneurysm thrombus. Biomechanics and Modeling in Mechanobiology **7**(2), 127–137 (Apr 2008)
8. Degroote, J.: Partitioned simulation of fluid-structure interaction. Archives of Computational Methods in Engineering **20**(3), 185–238 (Sep 2013)
9. Degroote, Joris and Haelterman, Robby and Annerel, Sebastiaan and Vierendeels, Jan: Coupling techniques for partitioned fluid-structure interaction simulations with black-box solvers. In: MpCCI User Forum, 10th, Proceedings. pp. 82–91. Fraunhofer Institute SCAI (2009)
10. Felippa, C.A., Park, K., Farhat, C.: Partitioned analysis of coupled mechanical systems. Computer Methods in Applied Mechanics and Engineering **190**(24), 3247–3270 (2001), advances in Computational Methods for Fluid-Structure Interaction
11. Fernández, M.A.: Coupling schemes for incompressible fluid-structure interaction: implicit, semi-implicit and explicit. SeMA Journal **55**(1), 59–108 (Sep 2011)
12. Han, D., Zhang, J., He, G., Griffith, B.P., Wu, Z.J.: A prestressed intracellular biomechanical model for the platelet to capture the disc-to-sphere morphological change from resting to activated state. International Journal of Computational Methods **19**(10), 2250021 (2022)
13. Hao, Y., Závodszky, G., Tersteeg, C., Barzegari, M., Hoekstra, A.G.: Image-based flow simulation of platelet aggregates under different shear rates. PLOS Computational Biology **19**(7), 1–20 (07 2023)

ICCS Camera Ready Version 2024
To cite this paper please use the final published version:
DOI: 10.1007/978-3-031-63783-4_5

14. Hecht, F.: New development in freefem++. J. Numer. Math. **20**(3-4), 251–265 (2012)
15. Huang, C.C., Shih, C.C., Liu, T.Y., Lee, P.Y.: Assessing the viscoelastic properties of thrombus using a solid-sphere-based instantaneous force approach. Ultrasound in Medicine & Biology **37**(10), 1722–1733 (2011)
16. Kadri, O.E., Chandran, V.D., Surblyte, M., Voronov, R.S.: In vivo measurement of blood clot mechanics from computational fluid dynamics based on intravital microscopy images. Computers in Biology and Medicine **106**, 1–11 (2019)
17. Küttler, U., Wall, W.A.: Fixed-point fluid–structure interaction solvers with dynamic relaxation. Computational Mechanics **43**(1), 61–72 (Dec 2008)
18. Lee, S., Jang, S., Park, Y.: Measuring three-dimensional dynamics of platelet activation using 3-d quantitative phase imaging. bioRxiv (2019)
19. Maas, S.A., Ellis, B.J., Ateshian, G.A., Weiss, J.A.: FEBio: Finite Elements for Biomechanics. Journal of Biomechanical Engineering **134**(1), 011005 (02 2012)
20. Matthies, H.G., Niekamp, R., Steindorf, J.: Algorithms for strong coupling procedures. Computer Methods in Applied Mechanics and Engineering **195**(17), 2028–2049 (2006)
21. Rugonyi, S., Bathe, K.: On the analysis of fully-coupled fluid flows with structural interactions - a coupling and condensation procedure. International Journal for Computational Civil and Structural Engineering **1**, 29–41 (01 2000)
22. Slaboch, C.L., Alber, M.S., Rosen, E.D., Ovaert, T.C.: Mechano-rheological properties of the murine thrombus determined via nanoindentation and finite element modeling. Journal of the Mechanical Behavior of Biomedical Materials **10**, 75–86 (2012)
23. Stalker, T.J., Traxler, E.A., Wu, J., Wannemacher, K.M., Cermignano, S.L., Voronov, R., Diamond, S.L., Brass, L.F.: Hierarchical organization in the hemostatic response and its relationship to the platelet-signaling network. Blood **121**(10), 1875–1885 (03 2013)
24. Storti, F., van de Vosse, F.N.: A continuum model for platelet plug formation, growth and deformation. International Journal for Numerical Methods in Biomedical Engineering **30**(12), 1541–1557 (2014)
25. Teeraratkul, C., Tomaiuolo, M., Stalker, T.J., Mukherjee, D.: Investigating clot-flow interactions by integrating intravital imaging with in silico modeling for analysis of flow, transport, and hemodynamic forces. Scientific Reports **14**(1), 696 (Jan 2024)
26. Trudnowski, R.J., Rico, R.C.: Specific gravity of blood and plasma at 4 and 37 °C. Clinical Chemistry **20**(5), 615–616 (05 1974)
27. Voronov, R.S., Stalker, T.J., Brass, L.F., Diamond, S.L.: Simulation of intrathrombus fluid and solute transport ssing in vivo clot structures with single platelet resolution. Annals of Biomedical Engineering **41**(6), 1297–1307 (Jun 2013)
28. Wang, W., Lindsey, J.P., Chen, J., Diacovo, T.G., King, M.R.: Analysis of early thrombus dynamics in a humanized mouse laser injury model. Biorheology **51**, 3–14 (2014), 1
29. Welsh, J.D., Stalker, T.J., Voronov, R., Muthard, R.W., Tomaiuolo, M., Diamond, S.L., Brass, L.F.: A systems approach to hemostasis: 1. The interdependence of thrombus architecture and agonist movements in the gaps between platelets. Blood **124**(11), 1808–1815 (09 2014)
30. Winterstein, A., Lerch, C., Bletzinger, K.U., Wüchner, R.: Partitioned simulation strategies for fluid–structure–control interaction problems by gauss–seidel formulations. Advanced Modeling and Simulation in Engineering Sciences **5**(1), 29 (Dec 2018)

ICCS Camera Ready Version 2024
To cite this paper please use the final published version:
DOI: 10.1007/978-3-031-63783-4_5